

THE EFFECTIVENESS OF FUZZY LOGIC CONTROL FOR PV PUMPING SYSTEM

A.TERKI*, A. MOUSSI, A. BETKA & N. TERKI

Electrical Engineering Department, University of Biskra, Algeria,
*terki_am1@yahoo.fr

ABSTRACT

This paper presents an optimal operation of a photovoltaic pumping system. An analysis by which the dynamic performances of a permanent magnet brushless DC (PMBLDC) motor is controlled through a hysteresis current loop and an outer speed loop with different controllers. The dynamics of the drive system with (PI) and a Fuzzy logic (FL) speed controllers are presented. In order to optimize the overall system efficiency, a maximum power point tracker is also used. Simulation is carried out by formatting the mathematical model for photovoltaic source, MPPT, motor and pump load. The results with FL speed controller show improvement in transient response of PMBLDC drive over conventional PI. The effectiveness of the FL controller is also demonstrated.

KEYWORDS: photovoltaic system, brushless DC motor, hysteresis controller, FL controller, optimization

1 INTRODUCTION

It is well known that the sun provides almost all the energy needed to support life. On average the earth receives about $1.2 \cdot 10^{15}$ KW of solar power. The challenge for sustainable future is to tap a tiny fraction of this energy to supply the relative modest demands of human activities. Probably the most elegant way known to do this is to convert it straight into electricity using solar cells. Due to the initial installation price, one has to properly size and optimize the system operation. Most of research work concentrate on the optimal use of the photovoltaic generators which exhaust about 60 to 80% of the global price depending on whether storage means are used or not. The PV systems can be operated as a stand-alone, hybrid or grid connected system. The first schemes found a wide application in remote regions to meet small, but essential electric power requirement such as water pumping systems [1][3]. Early studies have concentrated on ways of sizing, matching and adapting PV pumping systems since a proper match between the installed capacity with the insolated load is essential to optimize such installations. Various studies have been done on the choice of the drive system, which suits PV source, types of pumps to use and ways to control and optimize the whole system [12]. This was firmly related to the existing technologies. At the early stage, only DC motors were used to drive pumps. Direct coupling of series, shunt, and separately excited DC motor PV pumping systems were studied [4][7]. It was found that the overall performances are totally different of those obtained when these motors are connected to a constant voltage source. Recent implementation showed that the PM motors

are well suited for PV pumping [8][9][14]. They features high level dynamics, fast response, and high efficiency which lend them naturally pumping systems mainly for low power. Similar work was carried out later feeding motors through a DC/DC converter [6][7][9]. for a better adaptation of the load to the source. Steady state and starting current and torque ratios efficiency improvement, and control implementation were analyzed. The use of adaptation techniques not only optimizes the output power from the PV generator but also improves motor characteristics such as starting torque and steady state parameters. It is well known that conventional PI controller is the most widely used in industrial applications due to its simple control structure, easy design and low cost. However, it suffers from lower response, oscillation and larger overshoot. The design of fuzzy logic controllers is still practically performed with trial and error method which has prevent a wide diffusion of system controllers based on fuzzy set theory. Therefore, FL controllers are specially designed to control problems of non-linear, non stationary, or ill-defined systems. This paper presents a hysteresis current controller for optimal operation of a brushless PM DC motor PV pumping system with different controllers (PI and FL). Maximum power tracker is also included to optimize the PV generator efficiency as well. Mathematical models for individual blocks are presented and overall system efficiency is investigated. Simulation results and conclusion follow thereafter. The system mainly consists of the solar cell array generator, DC/DC converter, PMBLDC motor coupled to a centrifugal pump as show in figure 1

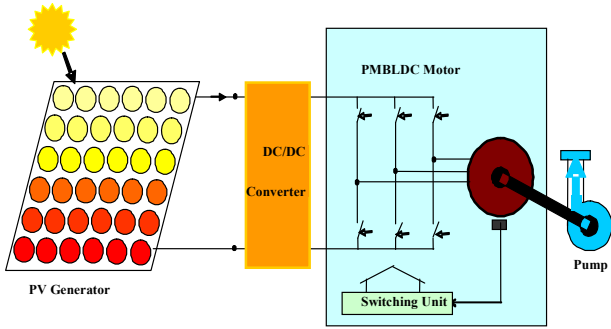


Figure1: The PV scheme structure

2 PV GENERATOR MODEL

The characteristic of the Photovoltaic generator can be presented by the following nonlinear equation [2][4]:

$$I = I_{sc} - I_o \left[\exp\left(\frac{V + R_s I}{V_{th}} \right) - 1 \right] - \frac{V + R_s I}{R_{sh}} \quad (1)$$

Where:

- I PVarray output current,
- R_{sh} PV array equivalent shunt resistance,
- I_{sc} PV array short circuit current,
- I_o PV array reverse saturation current,
- R_s PV array series resistance,
- V_{th} PV array thermal voltage.

The thermal voltage V_{th} and the reverse saturation current I_o are successively identified by [2, 6] :

$$V_{th} = \frac{(V_{op} + R_s I_{op} - V_{oc})}{\log\left(1 - \frac{I_{op}}{I_{sc}} \right)} \quad (2)$$

$$I_o = (I_{sc} - I_{op}) \exp\left(-\frac{(V_{op} + R_s I_{op})}{V_{th}} \right) \quad (3)$$

3 PERMANENT MAGNET BRUSH-LESS MOTOR MODEL

The simplified schematic of PMDC motor is shown in figure 2 Since this motor has trapezoidal electromotive force, the use of Park transform is not the best approach in modelling the machine. Instead the natural approach is used where the e.m.f is generated with respect to rotor position [8][9][10][12] . The operating sequences of the machine can be subdivided into six cycles with respect to rotor position. The electric of the motor can be described by [9][14][15].

$$V_{an} = R_i i_a + p \lambda_a + e_a \quad (4)$$

$$V_{bn} = R_i i_b + p \lambda_b + e_b \quad (5)$$

$$V_{cn} = R_i i_c + p \lambda_c + e_c \quad (6)$$

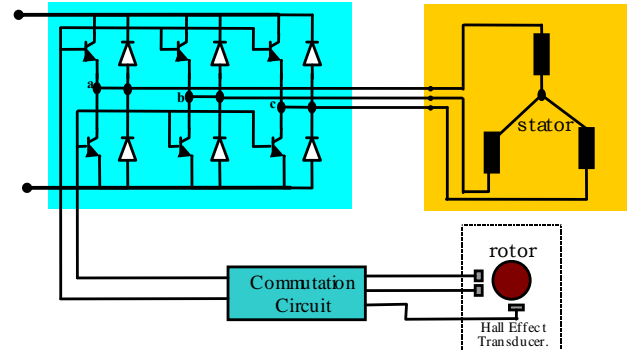


Figure 2: Brushless PMDC motor.

With

$$V_{an} = V_{a0} - V_{n0} \quad (7)$$

$$V_{bn} = V_{b0} - V_{n0} \quad (8)$$

$$V_{cn} = V_{c0} + V_{n0} \quad (9)$$

Where R: per phase stator resistance. $i_{a,b,c}$ and $\lambda_{a,b,c}$ are respectively phase currents of phases a, b and c and total flux linkage of a,b and c.p: Laplace operator. The flux expressions are given by the following equations:

$$\lambda_a = L_s i_a - M(i_b + i_c) \quad (10)$$

$$\lambda_b = L_s i_b - M(i_a + i_c) \quad (11)$$

$$\lambda_c = L_s i_c - M(i_a + i_b) \quad (12)$$

Where L_s : the self inductance and M : the mutual inductance.

$$\text{And } i_a + i_b + i_c = 0 \quad (13)$$

Therefore by substituting Eq.13 in Esq. 10, 11 and 12:

$$\lambda_a = i_a (L_s + M) \quad (14)$$

$$\lambda_b = i_b (L_s + M) \quad (15)$$

$$\lambda_c = i_c (L_s + M) \quad (16)$$

From the electrical equations 4, 5 and 6, the following system is obtained

$$\begin{bmatrix} V_{an} \\ V_{bn} \\ V_{cn} \end{bmatrix} = \begin{bmatrix} R & 0 & 0 \\ 0 & R & 0 \\ 0 & 0 & R \end{bmatrix} \begin{bmatrix} i_a \\ i_b \\ i_c \end{bmatrix} + p \begin{bmatrix} L_{eq} & 0 & 0 \\ 0 & L_{eq} & 0 \\ 0 & 0 & L_{eq} \end{bmatrix} \begin{bmatrix} i_a \\ i_b \\ i_c \end{bmatrix} + \begin{bmatrix} e_a \\ e_b \\ e_c \end{bmatrix} \quad (17)$$

With $L_{eq} = L_S + M$

From this system, the decoupled phase equations are obtained and the explicit current equations are given by:

$$p \begin{bmatrix} i_a \\ i_b \\ i_c \end{bmatrix} = \begin{bmatrix} 1/L_{eq} & 0 & 0 \\ 0 & 1/L_{eq} & 0 \\ 0 & 0 & 1/L_{eq} \end{bmatrix} \begin{bmatrix} V_{an} \\ V_{bn} \\ V_{cn} \end{bmatrix} - \begin{bmatrix} R & 0 & 0 \\ 0 & R & 0 \\ 0 & 0 & R \end{bmatrix} \begin{bmatrix} i_a \\ i_b \\ i_c \end{bmatrix} - \begin{bmatrix} e_a \\ e_b \\ e_c \end{bmatrix} \quad (18)$$

The mechanical part is expressed by the following equation:

$$J \frac{d\Omega}{dt} + B \Omega = T_e + T_r \quad (19)$$

With: T_e : electromagnetic torque.

T_r : Load torque

Ω : speed

J: moment of inertia

B: viscose friction coefficient

Neglecting the frictional coefficient and taking

$\Omega = \frac{W}{P}$ where P is the pole pairs number, (19) can written as:

$$\frac{dW}{dt} = P (T_e - T_r) / J \quad (20)$$

The developed torque can be expressed by

$$T_e = (e_a i_a + e_b i_b + e_c i_c) / W \quad (21)$$

And the angular position is expressed by

$$\frac{d\theta}{dt} = W \quad (22)$$

4 SPEED CONTROL

4.1 Classical PI controller

PI speed controller is widely used in industry due to its ease design and simple structure. The rotor speed $W(k)$ is compared with the reference speed $W_{ref}(k)$ and the resulting error is estimated at the nth sampling instant as:

$$e(k) = W(k) - W(k-1) \quad (23)$$

$$\Delta e(k) = e(k) - e(k-1) \quad (24)$$

The value of the torque reference is given by [1]:

$$T_{ref}(k) = T_{ref}(k-1) + K_p \Delta e(k) + K_i e(k) \quad (25)$$

Where $e(k-1)$ the speed error of previous interval is, $e(k)$ is the speed error of working interval. k_p and k_i are speed controller gains.

4.2 Fuzzy Logic Controller

Fuzzy logic permits to define control laws of any process starting from linguistic description of the control strategy to be adopted. Fuzzy logic uses controller is a rule-based controller; it consists of an input, processing, and output stages. The input or fuzzification stage maps instead of numerical variable linguistic ones, which are variables whose values (fuzzy subsets) are labels or sentences in a natural or artificial language[13].In a basic configuration of a fuzzy logic controller:

4.2.1 Fuzzification

or linguistic coding of in put variables, which transforms a given set of numerical inputs into fuzzy linguistic variables set composed of fuzzy subsets called also membership functions. The most common shape of membership functions is triangular, although trapezoids and bell curves are also used.

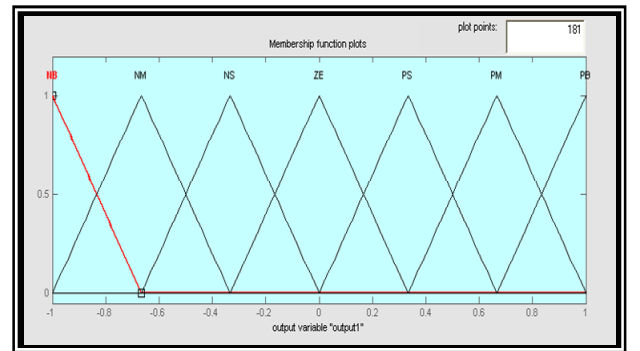


Figure 3: the membership functions

4.2.2 Inference fuzzy rules

Which contains a set of fuzzy rules in linguistic form as well as database which is a collection of expert control knowledge allowing the achievement of a fuzzy control objectives. This control rules base can be set up using IF-

THEN rules, based on expert experience and or engineering knowledge, and learning fuzzy rule-based system which has learning capabilities. There are several different ways to define the result of a rule, but one of the most common and simplest is the "max-min" inference method, in which the output membership function is given the truth value generated by the premise. The look up table for the input and output rules defined for seven linguistic variables (NB, NM, NS, ZE, PS, PM, PB) that stand for negative big, negative medium, negative small, zero, positive small, positive medium and positive big respectively is given in Table.1.

4.2.3 Defuzzification

Of the inference engine, which evaluates the rules based on a set of control actions for a given fuzzy inputs set. This operation converts the inferred fuzzy control action into a numerical value at the out- put. The results of all the rules that have fired are "defuzzified" to a crisp value by one of several methods. There are dozens in theory, each with various advantages and drawbacks. The "centroid" method is very popular, in which the "center of mass" of the result provides the crisp value. Another approach is the "height" method, which takes the value of the biggest contributor. The centroid method favors the rule with the output of greatest area, while the height method obviously favors the rule with the greatest output value.

Table 1 : The error and change of error

e Δe	NB	NM	NS	ZE	PS	PM	PB
NB	NB	NB	NB	NB	NM	NS	ZE
NM	NB	NM	NM	NM	NS	ZE	PS
NS	NB	NM	NS	NS	ZE	PS	PM
ZE	NB	NM	NS	ZE	PS	PM	PB
PS	NM	NS	ZE	PS	PM	PM	PB
PM	NS	ZE	PS	PM	PM	PB	PB
PB	ZE	PS	PM	PB	PB	PB	PB

5 CURRENT CONTROL

Several techniques can be used to control the phase current of the brushless PM DC motor. In this paper a hysteresis current controller is used. It has the major advantage of not requiring machine parameters to be known. However the commutation frequency is not constant. [12][13]. It depends on many factors such as the applied voltage, the back emf, hysteresis band ΔI...etc. Maximum value of commutation frequency is obtained at starting and is given by [11]:

$$F_{max} = U / 8L_s \Delta I \tag{26}$$

The commutations are obtained by comparing actual currents $i_{a,b,c}$ to a rectangular reference $i_{a,b,c}^*$ and by keeping them in hysteresis band ΔI. The commutation sequences of switches are summarised in the following table, Table 2.

Table2 :The commutation sequences of switches

Si $i_a < (i_a^* - \Delta I)$	T ₁ on	T ₄ off	V _a = U/2
Si $i_a > (i_a^* + \Delta I)$	T ₁ off	T ₄ on	V _a = -U/2
Si $i_b < (i_b^* - \Delta I)$	T ₂ on	T ₅ off	V _b = U/2
Si $i_b > (i_b^* + \Delta I)$	T ₂ off	T ₅ on	V _b = -U/2
Si $i_c < (i_c^* - \Delta I)$	T ₃ on	T ₆ off	V _c = U/2
Si $i_c > (i_c^* + \Delta I)$	T ₃ off	T ₆ on	V _c = -U/2

6 PUMP MODEL

The pump used is of centrifugal type which can be described by an aerodynamic load which is characterised by the following load equation:

$$T_1 = AW^2 \tag{27}$$

where A is the pump constant.

The head versus capacity H=f(Q) characteristics are shown for the pump for different speed values using the base seed data and the affinity laws, Figure 4.

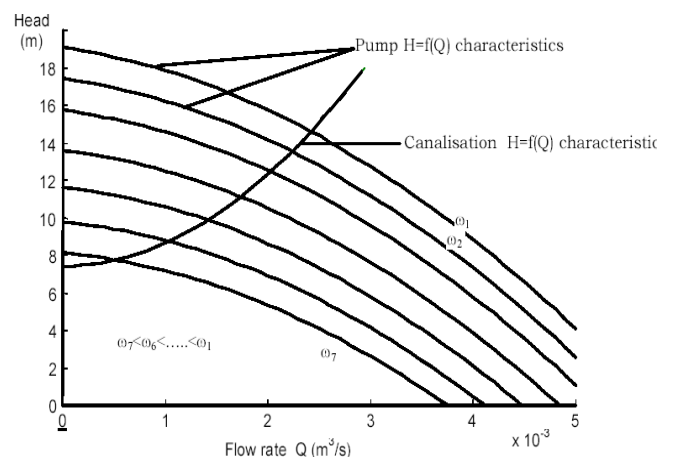


Figure 4: Multispeed family of pump head capacity curves showing operating points and canalization characteristic.

7 SIMULATION RESULTS

Using fourth order Runge-Kutta numerical resolution

method under Matlab, the overall system shown in Figure 5 was simulated. The system was first simulated without the hysteresis current controller and speed controllers. and then using them in order to see the effectiveness of this controller. Figure 6:a-b shows the simulation results without regulation, The phase current and torque high ripples are clearly seen. The torque pulsation are more than 15% of the average value. The source current is highly discontinuous and the speed presents an overshoot in addition to its moderate response. After, the speed and current regulations are introduced, results are shown in Figure 7 (regulation with PI controller) and Figure 8 (regulation with FL controller) the response current and torque ripples are distinctly reduced. Figure 7-8:a shows the current torque and speed responses of PMBLDC drive with no load where the current and torque decreased to zero value. The speed following the reference with overshoot in PI controller, so with FL controller, the speed converges to the reference value very quickly without any overshoot and with zero steady state error. The results under loading condition are shown in Figure 7-8:b it is shown that the proposed drive with FL controller is also capable of following the reference speed at best time response, zero steady state error and almost without any overshoot.

Figure 9 show a PV generator I-V and P-V characteristics, the generator output current, the drive speed and motor torque for solar insolation of $1000W/m^2$. It is seen that the maximum power is efficiently tracked, and motor performance are quiet good. At starting the current rises to the short circuit value of 4.82A with a time constant which depends on motor electrical parameters and decreases at the value of 4.41A corresponding to optimal current and optimal voltage of 175V. The corresponding maximum power of the PV generator is 772W. The final steady state speed of 300 rad/s is reached with no overshoot.

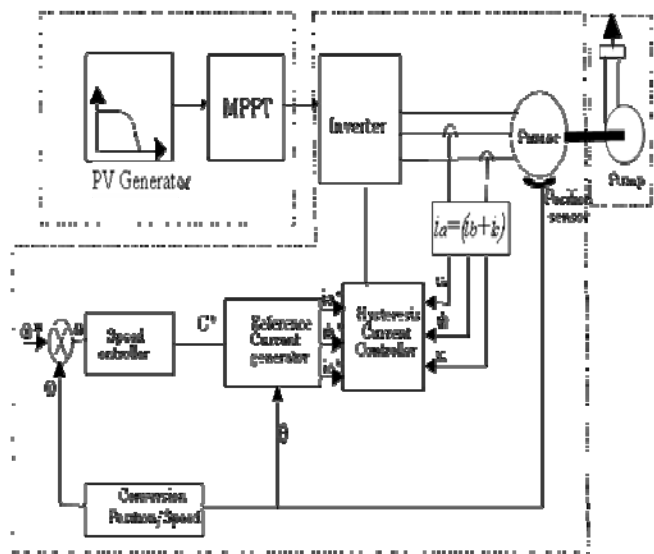
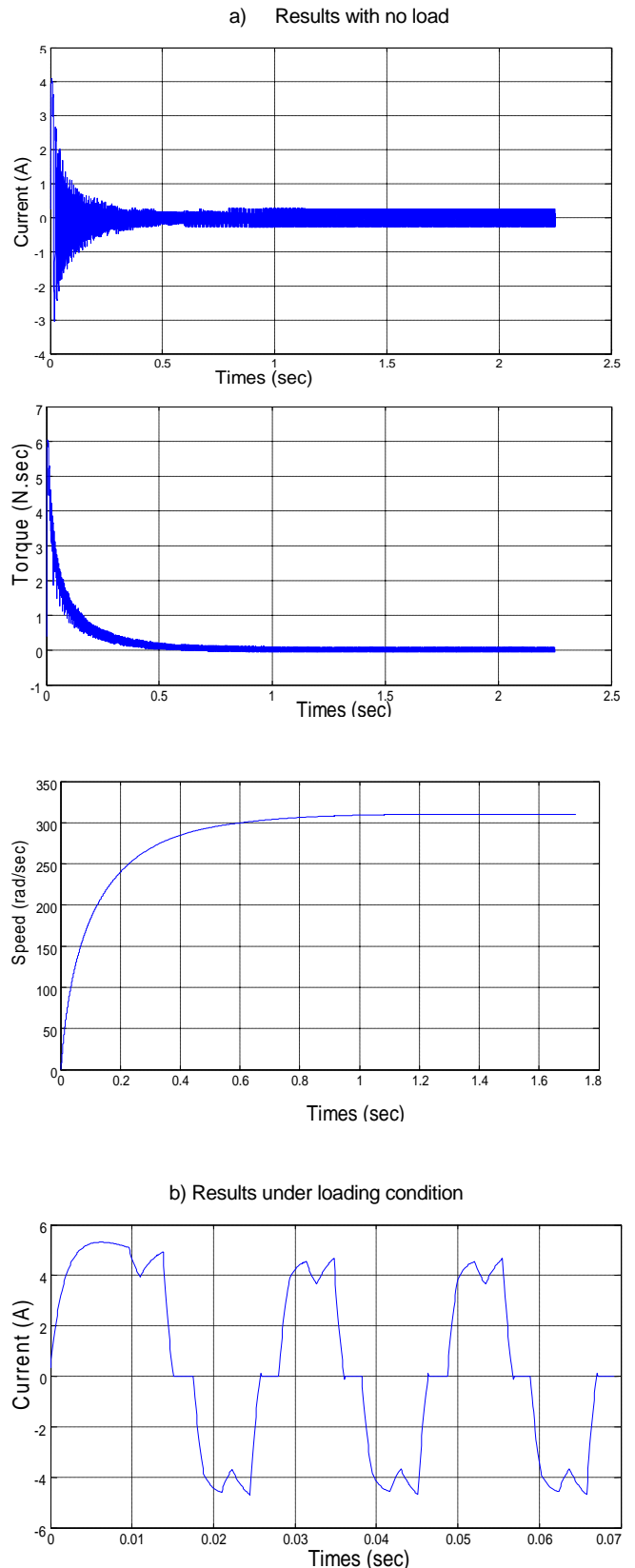
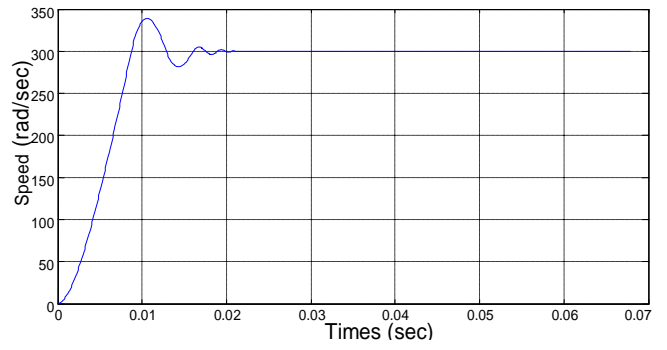
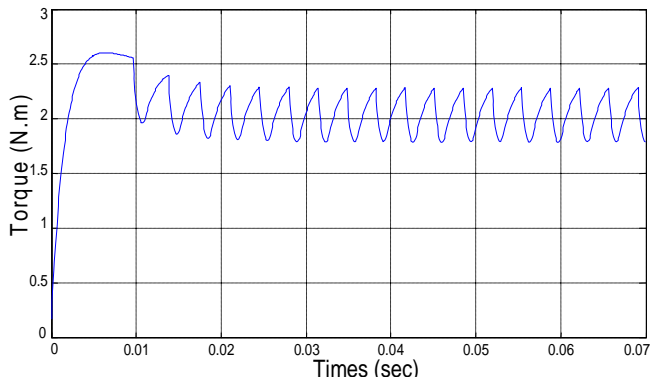


Figure 5: Overall system configuration





b) Results under loading condition

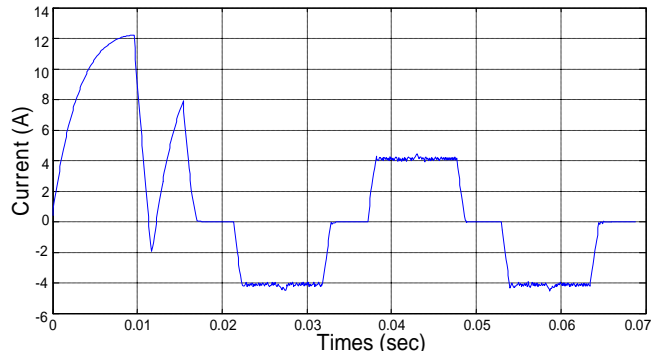
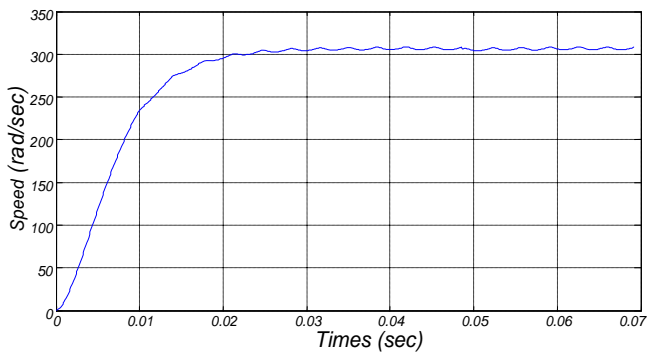


Figure 6: Simulation results without regulation

a) Results with no load

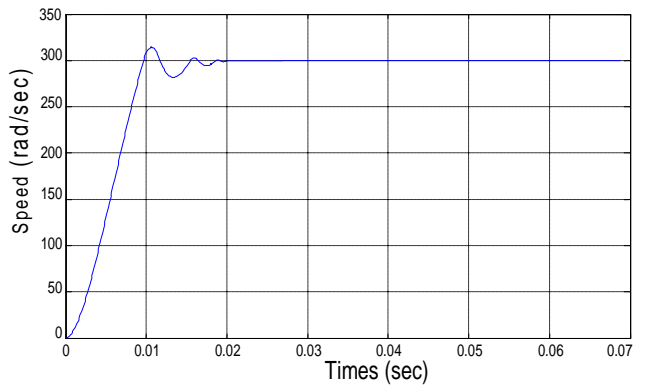
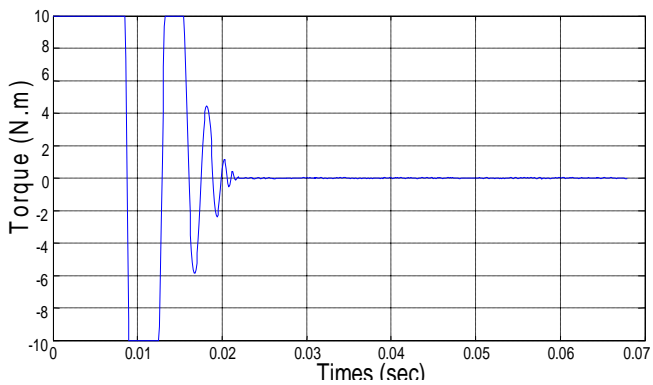
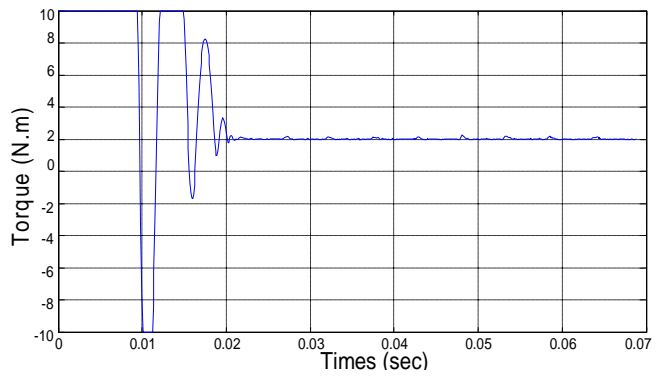
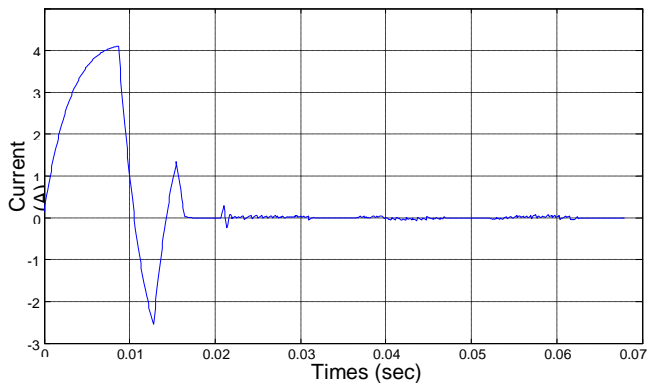


Figure 7: Simulation results with PI speed and hysteresis current controllers regulation

a) Results with no load

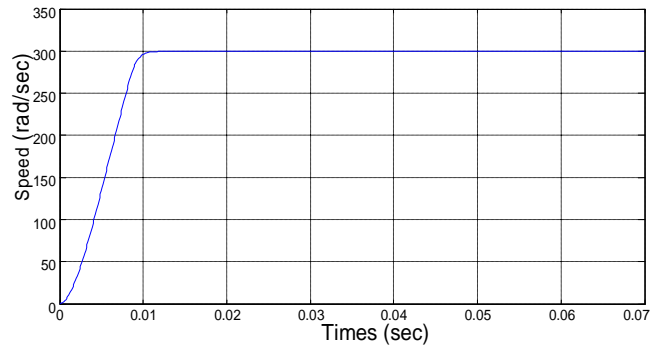
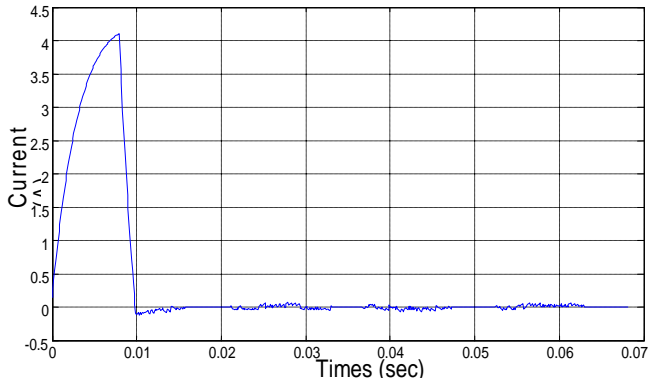
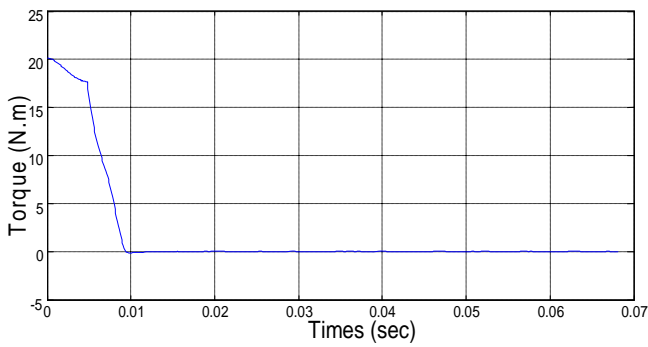
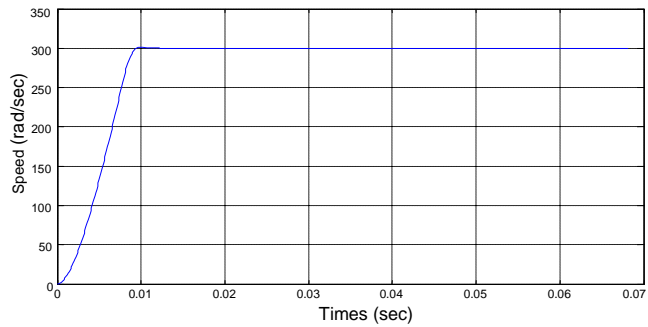
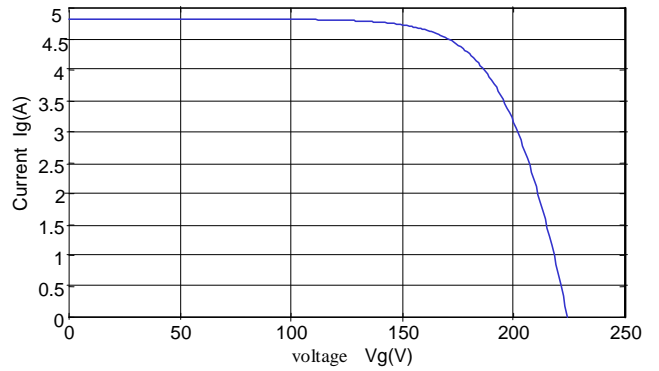


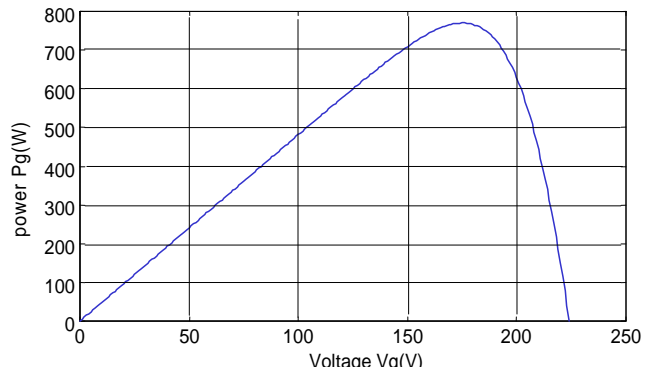
Figure 8: Simulation results with FL speed and hysteresis current controllers' regulation



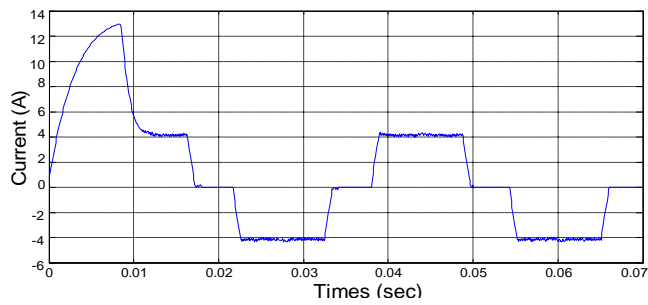
a) I,V Characteristics of photovoltaic Generator



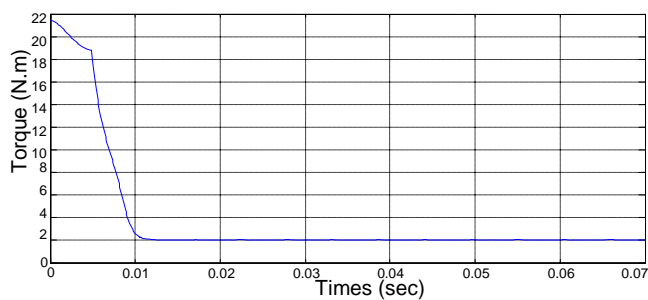
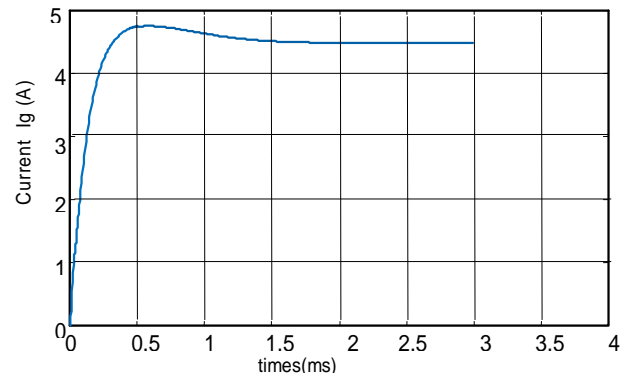
b) P,V Characteristics of photovoltaic Generator



b) Results under loading condition



c) Out put current of photovoltaic Generator



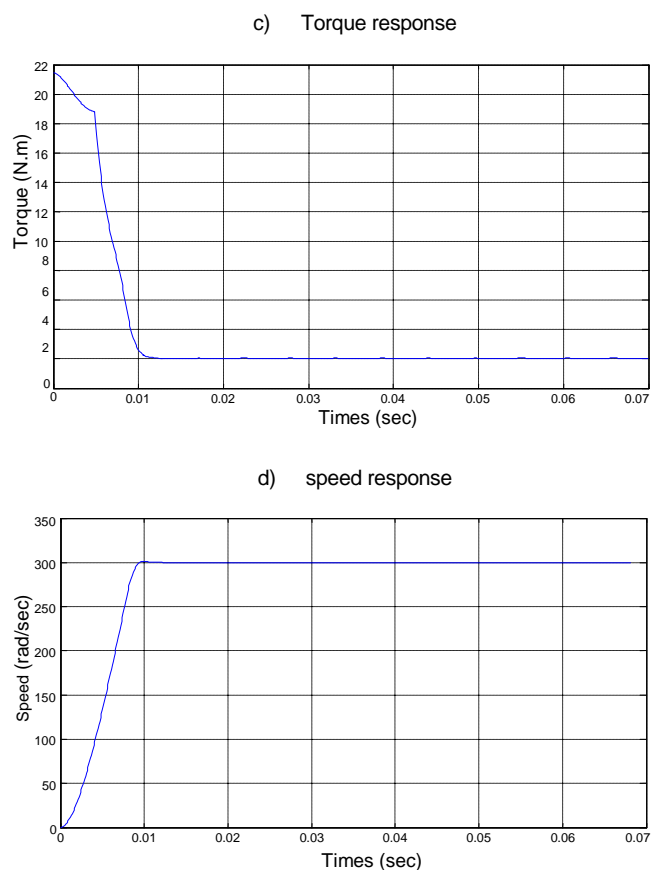


Figure 9: Simulation results for solar insolation 1000W/m^2

8 CONCLUSION

Performances of brushless PMDC motor connected to photovoltaic array and driving a centrifugal pump is investigated. The system was first studied without regulation then with a hysteresis controller and two types of speed controllers: classical PI and fuzzy logic (FL) at no load and under loading conditions. The dynamic behaviours of the drive system with both controllers were presented and compared. It was proved that for such complicated and nonlinear control system, the FL controller ensures much better dynamical properties.

APPENDIX

The PV generator, motor and pump used in this study have the following parameters:

PV generator Modules AEG-40.

(Temperature $T=25^\circ\text{C}$ and solar insolation $E=1000\text{W/m}^2$.)

Open circuit voltage	22.40 V
Short circuit current	2.410 A
Series resistance	0.450 Ω
Current temperature coefficient	0.06%/ C
Voltage temperature coefficient	0.40%/ C
Centrifugal pump	
Rated speed	3000 rev/min

Rated power	521 W
Flow rate	2.597 l/s
Head	14.11 m
Efficiency	69%
<i>Brushless DC motor</i>	
Rated power	690 W
Rated speed	690 W
Rated voltage	200-220V
Rated current	4.8 A
Per phase resistance	1 Ω
Per phase inductance	5 mH
Poles number	6
E.m.f constant	0.47

BIBLIOGRAPHIE

- [1] G. B. SHRERTHA, L. GOEL, "A Study On Optimal Sizing Of Stand Alone Photovoltaic Stations" IEEE Trans. on EC, Vol. 13, No. 4, 1998, pp: 373-377.
- [2] J. SAMIN and al. "Optimal sizing of Photovoltaic Systems in Varied Climates" Solar Energy, vol.6, No.2, 1997, pp: 97-107.
- [3] K. KALAITZAKIS "Optimal PV System Dimensioning with Obstructed Solar Radiation" Renewable Energy, Vol. 7, No. 1, pp: 51-56.
- [4] Z. ZINGE, "Optimum Operation of a Combined System pf a Solar Cell Array and a DC Motor", IEEE Trans. on PAS, Vol. PAS-100, No. 3, 1981, pp: 1193-1197.
- [5] J. APPELBAUM, "Starting and Steady State Characteristics of DC Motor Powered by Solar Cell Generator", IEEE Trans. on EC, Vol. 1, No. 1, 1986, pp: 17-25.
- [6] M. M. SAIED, "Matching of DC Motor to Photovoltaic generator for Maximum Daily Gross Mechanical Energy" IEEE Trans. on EC, Vol. 3, No. 3, 1988, pp: 465-471.
- [7] J. Appelbaum, M. S. Sarme, "The Operation of Permanent Magnet DC motors Powered by a Common Source of Solar Cells", IEEE Trans. on EC, Vol. 4, No. 4, 1989, pp: 635-642.
- [8] S. SINGER, "Starting Characteristics Of Direct Current Motors Powered By Solar Cells", IEEE Trans. on EC, Vol. 8, No. 1, 1993, pp: 47-52.
- [9] V. C. MUMMADI, "Steady State And Dynamic Performances Analysis Of PV Supplied DC Motors Fed From Intermediate Power Converter", Solar Energy Materials & Solar Cells, Vol-61, 2000, pp: 365-381.
- [10] S. R. BHAT, and al, "Performance Optimization of Induction Motor-Pump System Using Photovoltaic Energy Source", IEEE Trans. on IA, Vol. 23, No. 6, 1987, pp: 995-1000.
- [11] M. VEERACHARY, N. YADAIAH, "ANN Based Peak Power Tracking For PV Supplied Dc Motors", Solar Energy, Vol. 69, NO. 4, 2000, pp: 343-350.
- [12] T. HIYAMA, and al. "Neural Network Based Estimation Of Maximum Power Generation From PV Modules Using Environmental Information", IEEE Trans. on EC, Vol. 12, No. 3, 1997, pp: 241-247.

- [13] T. F. WU and al. "A Fuzzy-Logic-Controlled Single-Stage Converter for PV-Powered Lighting System Application", IEEE Trans. IE, Vol. 47, No. 2, 2000, pp: 287-296
- [14] C. L. P. SWAMY and al. "Dynamic Performance of a permanent Magnet Brushless DC Motor Powered by a PV Array for Water Pumping" Solar Energy Materials and Solar Cells, Vol. 36, 1995, pp: 187-200.
- [15] A. Betka, A. Attali " Optimization of a photovoltaic pumping system based on the optimal control theory" Solar Energy, Vol. 84, N°7, july2010, pp 1273-1283.